Propagation of acoustic waves in a slowly varying duct with multiple-scales potential flow using the multimodal formulation

Bruno Mangin, Majd Daroukh, Gwenael Gabard

Propagation of acoustic waves in a slowly varying duct with multiple-scales potential flow using the multimodal formulation

B. Mangin* and M. Daroukh†
DAAA, ONERA, Université Paris Saclay, F-92322 Châtillon, France

G. Gabard‡
Laboratoire d'Acoustique de l'Université du Mans (LAUM), UMR 6613, Institut d'Acoustique - Graduate School (IA-GS), CNRS, Le Mans Université, France

This paper presents a multimodal method applicable to the computation of the acoustic field in an axisymmetric duct with multiple-scales potential mean flow. The original three-dimensional set of equations is rearranged into a set of coupled one-dimensional equations by using the Fourier transform of the sound disturbances in the azimuthal direction and a projection on shifted Chebyshev polynomials in the radial direction. To keep the computation resources identical to that of the standard multimodal formulation (without flow), only the leading order effects of the mean flow are encapsulated using a multiple-scales approach. The formulation is verified using a finite-element method and is shown to give consistent results for modes propagating inside ducts with or without acoustic liners and in the presence of potential flows. This method can be easily adapted to take into account more complex flows and geometries.

I. Introduction

Despite the analytical and numerical advancements that enable us to assess guided wave problems, solving these problems efficiently has always been a major challenge in turbomachinery for complex cases (such as critical reflections [1], cut-off waves [2], etc.).

Analytical methods have been developed to solve these guided wave problems by introducing some simplifications on the geometry and the flow [3–8]. The basic idea behind all these studies is to dissociate the resolution in the privileged propagation direction, with assumptions on the axial shape of the wave, and in the transverse plane, using a modal representation. They offer results of first interest, but their domain of validity remains limited, and reflection and scattering phenomena cannot be accurately predicted. To overcome these difficulties, fully numerical simulations based on the linearized Euler equations (LEE), such as the finite-element methods (FEM), can be used. They allow to calculate precisely the solution to these propagation problems, but they do not take any advantage of their nature.

Combining the strength of both methodologies then naturally comes to mind to solve complex guided wave problems. Several studies have been conducted with that idea (see for example [9, 10]) and demonstrate that most of the complexity comes from the estimation of the shape of the acoustic fluctuations in the privileged propagation direction. Therefore, a method that would use the modal representation of the analytical methods but would numerically solve the axial shape of the wave problem would be very attractive. This idea is the basis of the multimodal method (MM), which consists in rearranging the acoustic problem in a set of coupled one-dimensional (1D) amplitude equations describing the evolution of the modes. This approach seems easy to implement, but two problems quickly emerge. First, the acoustic equation with evanescent modes is unstable, making it particularly difficult to solve. Then, the problem is not just an initial value problem since there is a strong coupling between the duct inlet and outlet. For two-dimensional (2D) ducts with varying cross-section, Pagneux *et al*. [11] overcame these difficulties by introducing an admittance matrix representing the medium's refraction and reflection index. They showed that the evolution of the admittance is driven by a Riccati equation which can be solved using a Magnus-Moebius scheme [12]. Afterwards, this method has been extended to three-dimensional (3D) ducts [13, 14] and appears to be extremely fast and accurate. However, multimodal models have been restricted to solutions of the Helmholtz equation with no mean flow.

*PhD student, Department of Aerodynamics, Aeroelasticity, and Aeroacoustics; bruno.mangin@onera.fr.
†Research Engineer, Department of Aerodynamics, Aeroelasticity, and Aeroacoustics; majd.daroukh@onera.fr.
‡Professor, LAUM; gwenael.gabard@univ-lemans.fr. Senior Member AIAA.

The current paper extends this methodology to compute acoustic fields in axisymmetric ducts with potential mean flows. However, using an exact solution for the mean flow would significantly increase the complexity and calculation time of the method. This issue is tackled by working on a simplified flow, which is found using multiple-scales assumptions. This allows to account for both the convection effect of the flow and the flow-induced scattering mechanisms at the first order, while maintaining the low calculation time of the standard multimodal formulation. The problem is solved by applying a Fourier transform in the azimuthal direction and a decomposition on Chebyshev polynomials in the radial direction of the perturbation equations.

The paper is organized as follows. Section II recalls the equations governing the flow and acoustic fields, which serve as a basis to construct our formulation. In Section III, our multimodal formulation with a potential flow is developed, and the basis of transverse modes is defined. Our numerical method is then validated against analytical solutions in section IV for an infinite uniform duct, and against FEM results in section V for a realistic engine geometry. Conclusions and discussions are finally provided in section VI.

II. Presentation of the problem

A. Governing equations

The acoustic propagation inside a 3D axisymmetric waveguide with an axially slowly varying annular cross-section is considered. Viscous and thermal effects are neglected. The vorticity is considered to be negligible, and no shock is expected. As a result, the flow is considered to be a perfect isentropic subsonic compressible irrotational gas flow.

In the following, all the parameters are transformed to be dimensionless: densities are normalized by a reference density ρ_∞, velocities are normalized by a reference sound speed c_∞, spatial dimensions by the typical duct radius R_∞, velocity potentials by $R_\infty c_\infty$, and pressures by $\rho_\infty c_\infty^2$. We begin by considering an associated cylindrical coordinate system (x, r, θ), with the associated eigenvectors $(\mathbf{e}_x, \mathbf{e}_r, \mathbf{e}_\theta)$, and by defining the slowly varying axial coordinate $X = \epsilon x$, where ϵ is a small parameter. The hub and tip radius slow variation can then be written $R_1(X)$ and $R_2(X)$. The analysis is done in the frequency domain and the characteristic pulsation of the source $\omega = 2\pi f$ is introduced, with f the frequency. The velocity vector, the density, the speed of sound and the pressure variables are written: $\tilde{\mathbf{v}} = \mathbf{V} + \mathrm{Re}(\mathbf{v}\, \mathrm{e}^{i\omega t}) = (U, V, W) + \mathrm{Re}((u, v, w)\, \mathrm{e}^{i\omega t})$, $\tilde{\rho} = D + \mathrm{Re}(\rho\, \mathrm{e}^{i\omega t})$, $\tilde{c} = C + \mathrm{Re}(c\, \mathrm{e}^{i\omega t})$, $\tilde{p} = P + \mathrm{Re}(p\, \mathrm{e}^{i\omega t})$ respectively. The capital letters denote the time-averaged values, and the lower-case letters represent the unsteady harmonic perturbations. The notations are identical to those used by Rienstra [15].

In this framework, the steady Euler equations for the mean flow are:

$$\begin{aligned} \nabla \cdot (D\mathbf{V}) &= 0, \\ D(\mathbf{V} \cdot \nabla)\mathbf{V} &= -\nabla P, \\ C^2 = \frac{\gamma P}{D} &= D^{\gamma - 1}, \end{aligned} \tag{1}$$

where γ is the ratio of specific heats. For the perturbation variables, the LEE are written:

$$\begin{aligned} i\omega\rho + \nabla \cdot (\rho\mathbf{V} + D\mathbf{v}) &= 0, \\ D(i\omega + \mathbf{V} \cdot \nabla)\mathbf{v} + D(\mathbf{v} \cdot \nabla)\mathbf{V} + \rho(\mathbf{V} \cdot \nabla)\mathbf{V} &= -\nabla p, \\ p &= C^2\rho. \end{aligned} \tag{2}$$

Hard-walled boundary conditions (BC) for the mean flow and lined wall BC for the acoustics [16] are considered at the hub and tip. They write:

$$\begin{aligned} \mathbf{V} \cdot \mathbf{n}_i &= 0 \\ (\mathbf{v} \cdot \mathbf{n}_i) &= \frac{1}{\mathrm{i}\omega}(\mathrm{i}\omega + \mathbf{V} \cdot \nabla - \mathbf{n}_i \cdot (\mathbf{n}_i \cdot \nabla\mathbf{V}))\frac{p}{Z_i}, \end{aligned} \tag{3}$$

at $r = R_i(X)$, with $\mathbf{n}_i$ the vector normal to the surface, Z_i the impedance of the liner and $i = 1, 2$.

B. Base flow

Following Rienstra [4], the mean flow equations are solved by assuming that the mean flow varies slowly with the axial coordinate X. Noting that $\partial A/\partial x = \epsilon \partial A/\partial X + O(\epsilon^2)$ for A any slowly varying variable, a reasoning on orders of

magnitude then shows that the flow variables take the form:

$$\begin{aligned}\mathbf{V}(X,r;\epsilon) &= U_0(X)\mathbf{e}_x + \epsilon V_1(X,r)\mathbf{e}_r + O(\epsilon^2),\\ [D,P,C](X,r;\epsilon) &= [D_0,P_0,C_0](X) + O(\epsilon^2).\end{aligned} \tag{4}$$

Injecting these expressions into equation (1) gives:

$$\begin{aligned}&\frac{1}{2}\left(\frac{F}{D_0(R_2^2-R_1^2)}\right)^2 + \frac{1}{\gamma-1}D_0^{\gamma-1} = E + O(\epsilon^2),\\ &U_0 = \frac{F}{D_0(R_2^2-R_1^2)} + O(\epsilon^2),\\ &P_0 = \frac{1}{\gamma}D_0^{\gamma} + O(\epsilon^2),\\ &C_0 = D_0^{(\gamma-1)/2} + O(\epsilon^2),\\ &V_1 = V_1^a(X)r + V_1^b(X)\frac{1}{r} = -\frac{F}{2D_0}\frac{\partial}{\partial X}\left(\frac{1}{R_2^2-R_1^2}\right)r + \frac{F}{2D_0}\frac{\partial}{\partial X}\left(\frac{R_1^2}{R_2^2-R_1^2}\right)\frac{1}{r} + O(\epsilon),\end{aligned} \tag{5}$$

where E and F are two constants (Bernoulli's constant and cross-sectional mass flow respectively). The numerical solution (e.g. calculated with a Newton algorithm) of the density's leading order allows to have access to the variation of all other mean flow quantities along the duct axis. In the rest of the paper, for concision reasons $(U,V,D,P,C) = (U,V^a r + V^b/r, D, P, C) = (U_0, \epsilon V_1^a r + \epsilon V_1^b/r, D_0, P_0, C_0)$.

III. Multimodal formulation with a potential flow

A. Modified wave equation

In standard multimodal formulation, the wave problem is solved using the acoustic pressure and the axial velocity. Trying to solve the equation on the pressure appears to be complex in a case with flow, therefore we prefer here to work with the velocity potential Φ such that $\mathbf{v} = \nabla\Phi$. In the cylindrical frame, the velocity potential satisfies, from equations (2) and (3):

$$\nabla\cdot(D\nabla\Phi) - D(i\omega + \mathbf{V}\cdot\nabla)\left[\frac{1}{C^2}(i\omega+\mathbf{V}\cdot\nabla)\Phi\right] = 0 \tag{6}$$

$$\mathrm{i}\omega(\nabla\Phi\cdot\mathbf{n}_i) = -(\mathrm{i}\omega + \mathbf{V}\cdot\nabla - \mathbf{n}_i\cdot(\mathbf{n}_i\cdot\nabla\mathbf{V}))\left[\frac{D}{Z_i}(\mathrm{i}\omega+\mathbf{V}\cdot\nabla)\Phi\right],\ \text{at } r = R_i(X) \text{ with } \mathrm{i} = 1,2. \tag{7}$$

Developing equation (6), removing the terms that are of order $O(\epsilon^2)$ or smaller, and introducing the variable $q = \dfrac{\partial\Phi}{\partial x}$ gives:

$$\frac{\partial}{\partial x}\left((1-M^2)q\right) = \left(-\Delta_\perp - k^2 - \frac{2\mathrm{i}}{C}\frac{\mathrm{d}C}{\mathrm{d}x}kM + 2\mathrm{i}k\frac{V}{C}\frac{\partial}{\partial r}\right)\Phi + \left(2\mathrm{i}kM + 2\frac{V}{C}M\frac{\partial}{\partial r}\right)q, \tag{8}$$

with $k = \omega/C$ the free-field wave number, $M = U/C$ the axial Mach number and $\Delta_\perp$ the transverse Laplacian operator. The equation (7) can be written as:

$$\begin{aligned}\mathrm{i}\omega(\nabla\Phi\cdot\mathbf{n}_i) = -&\left(\left(-\omega^2\frac{D}{Z_i} + \mathrm{i}\omega U\frac{\mathrm{d}}{\mathrm{d}x}\left(\frac{D}{Z_i}\right) + 2\mathrm{i}V\frac{D}{Z_i}\omega\frac{\partial}{\partial r} - \mathrm{i}\omega\frac{D}{Z_i}\frac{\partial V}{\partial r}\right)\Phi + \right.\\ &\left.\left(2\mathrm{i}\omega U\frac{D}{Z_i} + U\frac{\mathrm{d}}{\mathrm{d}x}\left(\frac{DU}{Z_i}\right) + 2UV\frac{D}{Z_i}\frac{\partial}{\partial r} - \frac{D}{Z_i}\frac{\partial V}{\partial r}U\right)q + \frac{D}{Z_i}U^2\frac{\partial q}{\partial x}\right).\end{aligned} \tag{9}$$

The next step consists in solving the acoustic variables on transverse cross-section modes such that the problem can be written as a set of first-order coupled differential equations. This basis is denoted here $(\varphi_j)_{j\in\mathbb{N}}$. As an example, the acoustic potential writes: $\Phi = \sum_j \Phi_j(x)\varphi_j(x,r,\theta)$. The equation (8) is multiplied by a test function φ_i^*, chosen to be

the complex conjugate of a basis function, and is integrated over a duct transverse surface S. Then by applying the divergence theorem, we obtain:

$$\begin{gathered}\int_S \varphi_i^* \frac{\partial}{\partial x}\left((1-M^2)q\right)\mathrm{d}S = \\ \int_S \left[\nabla_\perp \varphi_i^* \nabla_\perp \Phi + \varphi_i^*\left(-k^2 - \frac{2\mathrm{i}}{C}\frac{\mathrm{d}C}{\mathrm{d}x}kM + 2\mathrm{i}k\frac{V}{C}\frac{\partial}{\partial r}\right)\Phi + \varphi_i^*\left(2\mathrm{i}kM + 2\frac{V}{C}M\frac{\partial}{\partial r}\right)q\right]\mathrm{d}S - \int_\Lambda \varphi_i^* \nabla_\perp \Phi \cdot \mathrm{d}\Lambda.\end{gathered} \tag{10}$$

For numerical reasons, the equation is transformed by using the mass conservation to show as much as possible the hidden symmetries:

$$\begin{gathered}\frac{\mathrm{d}}{\mathrm{d}x}\left((1-M^2)\int_S \varphi_i^* \varphi_j dS q_n\right) - (1-M^2)\int_S \frac{\partial}{\partial x}(\varphi_i^*)\varphi_j \mathrm{d}S q_n = \\ \left[\int_S \nabla_\perp \varphi_i^* \nabla_\perp \varphi_j - k^2 \varphi_i^* \varphi_j - \mathrm{i}kM\left(\frac{1}{S}\frac{\mathrm{d}S}{\mathrm{d}x} + \frac{2}{C}\frac{\mathrm{d}C}{\mathrm{d}x}\right)\varphi_i^* \varphi_j - \mathrm{i}kM\frac{\partial}{\partial x}(\varphi_i^* \varphi_j) + \mathrm{i}k\frac{V}{C}\left(\varphi_i^*\frac{\partial}{\partial r}(\varphi_j) - \varphi_j\frac{\partial}{\partial r}(\varphi_i^*)\right)\mathrm{d}S\right. \\ \left. + \mathrm{i}kM\frac{\mathrm{d}}{\mathrm{d}x}\left(\int_S \varphi_i^* \varphi_j \mathrm{d}S\right)\right]\Phi_n \\ + \left[\int_S 2\mathrm{i}kM\varphi_i^* \varphi_j + \frac{VM}{C}\left(\varphi_i^*\frac{\partial}{\partial r}(\varphi_j) - \varphi_j\frac{\partial}{\partial r}(\varphi_i^*)\right) - M^2\frac{1}{S}\frac{\mathrm{d}S}{\mathrm{d}x}\varphi_i^* \varphi_j \mathrm{d}S\right] q_n - \int_\Lambda \varphi_i^* \nabla\Phi \cdot \mathrm{d}\Lambda.\end{gathered} \tag{11}$$

When the acoustic boundary is hard-walled, $\int_\Lambda \varphi_i^* \nabla\Phi \cdot \mathrm{d}\Lambda = 0$. Otherwise the equation (9) is injected into the previous equation. This leads to new equations governing the axial variation, which accounts for both the BC and the propagation operator:

$$\left(\begin{pmatrix} \mathcal{A}_{11} & 0 \\ 0 & \mathcal{A}_{22} \end{pmatrix} + \begin{pmatrix} 0 & 0 \\ 0 & \mathcal{B}_{22} \end{pmatrix}\right)\frac{\mathrm{d}}{\mathrm{d}x}\begin{pmatrix} \Phi_n \\ q_n \end{pmatrix} = \left(\begin{pmatrix} \mathcal{M}_{11} & \mathcal{M}_{12} \\ \mathcal{M}_{21} & \mathcal{M}_{22} \end{pmatrix} + \begin{pmatrix} 0 & 0 \\ \mathcal{N}_{21} & \mathcal{N}_{22} \end{pmatrix}\right)\begin{pmatrix} \Phi_n \\ q_n \end{pmatrix}, \tag{12}$$

with:

$$\begin{aligned}
\mathcal{A}_{11} &= \mathcal{A}_{22} = \mathcal{M}_{12} = (1-M^2)A_{ij}, \\
\mathcal{M}_{11} &= -(1-M^2)B_{ij}, \\
\mathcal{M}_{21} &= D_{ij} - k^2 A_{ij} - \mathrm{i}kM\left(\left(\frac{1}{S}\frac{\mathrm{d}S}{\mathrm{d}x} + \frac{2}{C}\frac{\mathrm{d}C}{\mathrm{d}x}\right)A_{ij} - \frac{\mathrm{d}}{\mathrm{d}x}\left(A_{ij}\right)\right) + \mathrm{i}k((C_{ij} - C_{ij}^*) - M(B_{ij} + B_{ij}^*)), \\
\mathcal{M}_{22} &= (1-M^2)B_{ij}^* - \frac{\mathrm{d}}{\mathrm{d}x}\left((1-M^2)A_{ij}\right) + 2\mathrm{i}kMA_{ij} + M(C_{ij} - C_{ij}^*) - \frac{M^2}{S}\frac{\mathrm{d}S}{\mathrm{d}x}A_{ij}, \\
\mathcal{B}_{22} &= \frac{\mathrm{i}D}{\omega}U^2 P_{ij}, \\
\mathcal{N}_{21} &= -\frac{\mathrm{i}D}{\omega}\left(\left(-\omega^2 + \mathrm{i}\frac{U}{D}\frac{\mathrm{d}D}{\mathrm{d}x}\omega\right)P_{ij} + \mathrm{i}U\omega Q_{ij} + 2\mathrm{i}\omega R_{ij} - \mathrm{i}\omega S_{ij}\right), \\
\mathcal{N}_{22} &= -\frac{\mathrm{i}D}{\omega}\left(U^2 T_{ij} + \left(2\mathrm{i}\omega U + \frac{U}{D}\frac{\mathrm{d}(DU)}{\mathrm{d}x}\right)P_{ij} + U^2 Q_{ij} + 2UR_{ij} - US_{ij}\right),
\end{aligned} \tag{13}$$

and where * denotes the adjoint operator. The above matrices are defined by:

$$
\begin{aligned}
A_{ij} &= \int_S \varphi_i^* \varphi_j \mathrm{d}S, \qquad B_{ij} = \int_S \varphi_i^* \frac{\partial \varphi_j}{\partial x} \mathrm{d}S, \\
C_{ij} &= \int_S \frac{V}{C} \varphi_i^* \frac{\partial \varphi_j}{\partial r} \mathrm{d}S, \quad D_{ij} = \int_S \nabla_\perp \varphi_i^* \nabla_\perp \varphi_j \mathrm{d}S, \\
P_{ij} &= \int_0^{2\pi} \left(R_2/Z_2 \ (\varphi_i^* \varphi_j)\big|_{r=R_2} - R_1/Z_1 \ (\varphi_i^* \varphi_j)\big|_{r=R_1} \right) \mathrm{d}\theta, \\
Q_{ij} &= \int_0^{2\pi} \left(R_2 \frac{\mathrm{d}1/Z_2}{\mathrm{d}x} \ (\varphi_i^* \varphi_j)\big|_{r=R_2} - R_1 \frac{\mathrm{d}1/Z_1}{\mathrm{d}x} \ (\varphi_i^* \varphi_j)\big|_{r=R_1} \right) \mathrm{d}\theta, \\
R_{ij} &= \int_0^{2\pi} \left(R_2/Z_2 \left(V \varphi_i^* \frac{\partial \varphi_j}{\partial r} \right)\Big|_{r=R_2} - R_1/Z_1 \left(V \varphi_i^* \frac{\partial \varphi_j}{\partial r} \right)\Big|_{r=R_1} \right) \mathrm{d}\theta, \\
S_{ij} &= \int_0^{2\pi} \left(R_2/Z_2 \left(\frac{\partial V}{\partial r} \varphi_i^* \varphi_j \right)\Big|_{r=R_2} - R_1/Z_1 \left(\frac{\partial V}{\partial r} \varphi_i^* \varphi_j \right)\Big|_{r=R_1} \right) \mathrm{d}\theta, \\
T_{ij} &= \int_0^{2\pi} \left(R_2/Z_2 \left(\varphi_i^* \frac{\partial \varphi_j}{\partial x} \right)\Big|_{r=R_2} - R_1/Z_1 \left(\varphi_i^* \frac{\partial \varphi_j}{\partial x} \right)\Big|_{r=R_1} \right) \mathrm{d}\theta.
\end{aligned}
\tag{14}
$$

The matrices $(P_{ij}, Q_{ij}, R_{ij}, S_{ij}, T_{ij})$ are associated with the radial boundary conditions and characterize the attenuation brought by the liner. In the case of an hard-walled duct, all these matrices are equal to zero.

B. Axial integration and boundary conditions

Equation (12) is unstable and cannot be integrated directly because of evanescent modes [1]. The multimodal method allows to solve this issue by defining an admittance matrix Y such that $q_n(x) = Y(x)\Phi_n(x)$. This admittance links the potential and its derivative and is therefore characteristic of the reflection and refraction index of the medium (Poincaré–Steklov operator). A new stable equation, called the Riccati equation, is obtained for this matrix:

$$
\frac{\mathrm{d}Y}{\mathrm{d}x} = -Y\mathcal{A}_{11}^{-1}\mathcal{M}_{11} - Y\mathcal{A}_{11}^{-1}\mathcal{M}_{12}Y + (\mathcal{A}_{22} + \mathcal{B}_{22})^{-1}(\mathcal{M}_{21} + \mathcal{N}_{21}) + (\mathcal{A}_{22} + \mathcal{B}_{22})^{-1}(\mathcal{M}_{22} + \mathcal{N}_{22})Y, \tag{15}
$$

and is solved using a Magnus-Moebius scheme [1, 12].

The solving allows assessing the value of the admittance inside the duct given an initial value Y_e, called the radiation condition. Many techniques are possible to define the latter. Let us define it such that the duct ends in an infinitely long uniform duct with only outgoing waves. In such a duct, all the global variables do not vary axially, and therefore the admittance is a fixed point of the Riccati equation. The goal is here to find this fixed point. This is done by using the analytical expressions of the infinite uniform duct case. The solution is written using a summation of modes over the cross-section that propagate or decay exponentially with the axial distance:

$$
\begin{pmatrix} \Phi_n(x) \\ q_n(x) \end{pmatrix} = \sum_i \alpha_i \begin{pmatrix} w_{i1} \\ w_{i2} \end{pmatrix} e^{\mathrm{i}\lambda_i x}, \tag{16}
$$

where $w_{i1/2}$ are eigenvectors representing the weight associated with the distribution over the cross-sectional basis functions φ_i, λ_i are the associated axial wavenumbers and α_i are constants. By injecting the expression (16) into the propagation equation (12), and by using the basis properties of the eigenvectors, the following eigenvalue problem is obtained:

$$
\mathrm{i}\lambda_i \begin{pmatrix} \mathcal{A}_{11} & 0 \\ 0 & \mathcal{A}_{22} + \mathcal{B}_{22} \end{pmatrix} \begin{pmatrix} w_{i1} \\ w_{i2} \end{pmatrix} = \begin{pmatrix} \mathcal{M}_{11} & \mathcal{M}_{12} \\ \mathcal{M}_{21} + \mathcal{N}_{21} & \mathcal{M}_{22} + \mathcal{N}_{22} \end{pmatrix} \begin{pmatrix} w_{i1} \\ w_{i2} \end{pmatrix}, \tag{17}
$$

Here, the solution is split into forward and backward waves based on the quadrants of the imaginary plane in which their associate eigenvalue lies. This allows, for example, to construct the forward matrix $\begin{pmatrix} \Phi_{n+} \\ q_{n+} \end{pmatrix} \propto \begin{pmatrix} W_{1+} \\ W_{2+} \end{pmatrix} e^{\Lambda_+ x}$ with $\begin{pmatrix} W_{1+} \\ W_{2+} \end{pmatrix} = \begin{pmatrix} w_{11}, ..., w_{n1} \\ w_{12}, ..., w_{n2} \end{pmatrix}$ and $\Lambda_+ = diagonal(i\lambda_1, ..., i\lambda_n)$ and where $\lambda_1, ..., \lambda_n$ and $w_{11/2}, ..., w_{n1/2}$ are the

eigenvalues and eigenvectors associated to forward waves. The backward Y_- and forward Y_+ admittances are introduced, and link the backward and forward modes respectively: $q_{n+} = Y_+\Phi_{n+}$, $q_{n-} = Y_-\Phi_{n-}$.

At the end of the duct, the waves only propagate forwards ($Y_e = Y_+$). The expression of the admittance matrix is then straightforward at the duct exit and writes:

$$Y_e = W_{2+}W_{1+}^{-1} = W_{1+}\Lambda_+W_{1+}^{-1} \tag{18}$$

When the transverse eigenmode basis is used (see section III.D.1 for hard-walled duct), the matrix W_{1+} is the identity matrix and the admittance matrix is a diagonal matrix with the axial wavenumbers as the diagonal terms. Otherwise, W_{1+} is the transfer matrix from the latter basis to the chosen basis.

Now that the admittance matrix is defined at the duct exit, the admittance matrix can be computed everywhere inside the duct by integrating equation (15).

C. Injection of a mode

The only thing left to do is to inject a source at the duct entrance, which consists in forcing a potential distribution on the chosen basis. However, the only known wave is the outgoing one generated by the acoustic source, noted Φ_+. If no reflection is expected inside the duct, this can be the value kept for the imposed potential Φ_n. Nevertheless, apart from rare cases, there are always waves travelling in the opposite direction, noted Φ_-, due to geometrical or flow reflections.

Let us define the reflection matrix $\mathcal{R}$ such as $\Phi_- = \mathcal{R}\Phi_+$. To obtain the reflection matrix $\mathcal{R}$ from the calculated admittance matrix Y, the acoustic potential is decomposed at the entry into a right and left propagating wave as:

$$\Phi_n = \Phi_+ + \Phi_- \text{ and } q_n = q_+ + q_-. \tag{19}$$

Using the computed admittance at the entrance and continuity conditions for the acoustic potential field and its axial derivative, the following relation is obtained:

$$Y(\Phi_+ + \Phi_-) = Y_+\Phi_+ + Y_-\Phi_-, \tag{20}$$

with $Y_{+/-}$ corresponding to the admittance matrix associated to the waves propagating forwards or backwards at the entrance. Since the previous relation is true for any injected field Φ_+, we obtain $\mathcal{R} = (Y - Y_-)^{-1}(Y_+ - Y)$ and the forced potential is $(I_n + \mathcal{R})\Phi_+$, with I_n the identity matrix.

Finally, using equation (11), the potential field inside the whole duct is obtained as the solution of:

$$\frac{\mathrm{d}\Phi_n}{\mathrm{d}x} = \left(\mathcal{A}_{11}^{-1}\mathcal{M}_{11} + \mathcal{A}_{11}^{-1}\mathcal{M}_{12}Y\right)\Phi_n. \tag{21}$$

D. Transverse mode basis

1. Standard hard-walled transverse mode basis

If a random basis is chosen for the φ_j, computing all the matrices given in equation (12) would be time-consuming and the method would not bring a significant gain compared to a fully numerical code. Therefore, the idea is to have a basis that gives us an analytical expression of the integrals of equation (14). Most multimodal studies [1, 11, 13, 17] use standard basis functions composed of local hard-walled transverse eigenmodes, solutions to the following eigenvalue problem:

$$-\Delta_\perp\varphi_j = \alpha^2\varphi_j, \tag{22}$$

$$\frac{\partial\varphi_j}{\partial r} = 0, \text{ at } r = R_i(X) \text{ with i} = 1, 2. \tag{23}$$

In our case, we associate a couple $(m, n) \in (\mathbb{Z}, \mathbb{N})$ to each index j such that the basis functions $\varphi_j = \varphi_{mn}$ are written [4]:

$$\varphi_{mn} = \frac{[\mathrm{J}_m(\alpha_{mn}r) + \Gamma\mathrm{Y}_m(\alpha_{mn}r)]\,\mathrm{e}^{-\mathrm{i}m\theta}}{\sqrt{2\pi\displaystyle\int_{R_1}^{R_2}[\mathrm{J}_m(\alpha_{mn}r) + \Gamma\mathrm{Y}_m(\alpha_{mn}r)]^2\,r\mathrm{d}r}}, \tag{24}$$

with m the azimuthal order, n the radial order, J_m and Y_m the m^{th}-order Bessel function of the first kind and second kind respectively and where the term Γ writes:

$$\Gamma = -\frac{\mathrm{J}'_m(\alpha_{mn}R_2)}{\mathrm{Y}'_m(\alpha_{mn}R_2)} = -\frac{\mathrm{J}'_m(\alpha_{mn}R_1)}{\mathrm{Y}'_m(\alpha_{mn}R_1)}. \tag{25}$$

As there is no possible coupling between different circumferential Fourier modes, we consider that the value of the azimuthal wavenumber m is fixed. In the following, no distinction is therefore made between j and n.

For a hard-walled duct, this basis has three major advantages: 1) an analytical expression of both A_{ij} and D_{ij} is known, 2) it gives an exact analytical solution of the acoustic field in regions without scattering, and 3) it is a complete basis, which means that the exact solution can be recovered if a sufficient number of modes is considered. However, this basis presents a major weakness because it is ill-posed at the wall level for sloped walls. Indeed, the derivatives of all basis functions are equal to zero at the wall which leads to vertical isobars that do not fulfill the acoustic boundary condition given by equation (3). This issue can be overcome by adding a non-physical supplementary Dirichlet mode inside the modal basis [14]. This solves the boundary problem, but this supplementary mode is case dependent, and it appears unlikely to have a universal one to solve the BC issue.

Note that the matrices of equation (14) can be classified into two categories when this basis is used for hard-walled ducts. Indeed, in this case, the matrices $A_{ij} = \delta_{ij}$ and $D_{ij} = \alpha_i^2\delta_{ij}$ are diagonal and represent the isolated mode propagation. On the opposite, the matrices B_{ij} and C_{ij} have non-diagonal terms that are equal to zero only when there is no wall variation. Moreover, C_{ij} is only non-zero when there is a non-zero flow. Therefore, the matrix B_{ij} is related to geometrical scattering while the matrix C_{ij} is linked to flow-induced scattering mechanisms. These three mechanisms are fully dissociated and can be investigated separately, allowing for a better physical understanding of the problem. All these phenomena can be dissociated because the chosen mean flow can be used to form an adiabatic invariant of the slowly varying mode and is not just an ad-hoc mean flow [4].

Note that the above reasoning could be done with transverse lined functions, but the equations need to be rearranged. In particular, some manipulations have to be done on the BC matrices and D_{ij} to dissociate the diagonal matrix $\alpha_i^2\delta_{ij}$ associated with the mode self-propagation from the scattering matrix.

2. Optimized transverse mode basis

Another method is proposed to overcome the wall boundary condition issue in the current paper. A Fourier transform again represents the acoustic field in the circumferential direction, while a set of polynomials is used in the radial direction. The polynomials have the advantage of being infinitely differentiable functions and are extremely fast to compute. The condition for these polynomials is that their derivative needs to be non zero at the wall to overcome the previously cited difficulty. Chebyshev functions are used in the current method since they have good convergence properties [7, 18, 19] . Considering this, at each basis function index j, we associated a couple $(m, p) \in (\mathbb{Z}, \mathbb{N})$ such that $\varphi_j = \varphi_p^m = T_p\left(\frac{r - R_1}{R_2 - R_1}\right)e^{-\mathrm{i}m\theta}$, with T_p the shifted Chebyshev polynomial of the first kind of order p and m the azimuthal wavenumber.

However, this choice displays a new issue: in the case of circular ducts ($R_1 = 0$), the matrix D_{ij} is not defined with this basis. Two types of solutions are proposed to solve this issue and are given below:

1) Separate the annular and circular resolution. In the circular case, a physical constraint on the coefficients of Fourier expansions in cylindrical coordinates is used [20]. This constraint imposes, for continuity reasons, that the radial functions should have the shape of $\varphi_p^m = r^{|m|}f_p(r)e^{-\mathrm{i}m\theta}$. A first intuitive idea would be to choose f_p to be a Chebyshev polynomial. However, this would imply important calculation resources since all the previous integrals should be computed for each azimuthal component. So for all m, a radial basis function of the form $\varphi_p^m = r^{\min(|m|,1)}T_p(r/R_2)e^{-\mathrm{i}m\theta}$ with T_p a Chebyshev polynomial is chosen. With this choice, the radial part of the basis functions is independent of the azimuthal order for $|m| > 0$ and all the integrals of equation (14) are defined.
2) Replace the R_1 value with a small non-zero constant in the case of a circular duct. This choice allows for a one-way calculation that avoids a junction between the annular and circular parts.

The second solution is the one chosen in this paper. There is again no possible coupling between different circumferential Fourier modes. Therefore we consider that the value of the azimuthal wavenumber m is fixed, and, in the rest of the paper, no distinction is made between φ_p^m and T_p. This choice allows deriving the expressions of the matrices given in

equation (14):

$$
\begin{aligned}
A_{ij} &= 2\pi\left((R_2-R_1)^2\int_0^1 T_i(r)T_j(r)r\mathrm{d}r + R_1(R_2-R_1)\int_0^1 T_i(r)T_j(r)\mathrm{d}r\right),\\
B_{ij} &= 2\pi\left((R_1-R_2)\frac{\mathrm{d}(R_2-R_1)}{\mathrm{d}x}\int_0^1 T_i(r)T_j'(r)r^2\mathrm{d}r + \frac{\mathrm{d}(R_1^2-R_2R_1)}{\mathrm{d}x}\int_0^1 T_i(r)T_j'(r)r\mathrm{d}r - R_1\frac{\mathrm{d}R_1}{\mathrm{d}x}\int_0^1 T_i(r)T_j'(r)\mathrm{d}r\right),\\
C_{ij} &= 2\pi\frac{V^a}{C}\left((R_2-R_1)^2\int_0^1 T_i(r)T_j'(r)r^2\mathrm{d}r + 2(R_2-R_1)R_1\int_0^1 T_i(r)T_j'(r)r\mathrm{d}r + R_1^2\int_0^1 T_i(r)T_j'(r)\mathrm{d}r\right)\\
&\quad + 2\pi\frac{V^b}{C}\left(\int_0^1 T_i(r)T_j'(r)\mathrm{d}r\right),\\
D_{ij} &= 2\pi\left(\int_0^1 T_i'(r)T_j'(r)r\mathrm{d}r + \frac{R_1}{R_2-R_1}\int_0^1 T_i'(r)T_j'(r)\mathrm{d}r + m^2\int_0^1 \frac{1}{r+\dfrac{R_1}{R_2-R_1}}T_i(r)T_j(r)\mathrm{d}r\right),\\
P_{ij} &= 2\pi(R_2/Z_2T_i(1)T_j(1) - R_1/Z_1T_i(0)T_j(0)),\\
Q_{ij} &= 2\pi\left(R_2\frac{\mathrm{d}(1/Z_2)}{\mathrm{d}x}T_i(1)T_j(1) - R_1\frac{\mathrm{d}(1/Z_1)}{\mathrm{d}x}T_i(0)T_j(0)\right),\\
R_{ij} &= \frac{2\pi}{R_2-R_1}\left(\left(V^aR_2^2+V^b\right)/Z_2\;T_i(1)T_j'(1) - \left(V^aR_1^2+V^b\right)/Z_1\;T_i(0)T_j'(0)\right),\\
S_{ij} &= 2\pi\left(R_2/Z_2\left(V^a-\frac{V^b}{R_2^2}\right)T_i(1)T_j(1) - R_1/Z_1\left(V^a-\frac{V^b}{R_1^2}\right)T_i(0)T_j(0)\right),\\
T_{ij} &= 2\pi\left(\frac{-R_2}{(R_2-R_1)Z_2}\frac{\mathrm{d}R_2}{\mathrm{d}x}T_i(1)T_j'(1) - \frac{-R_1}{(R_2-R_1)Z_1}\frac{\mathrm{d}R_1}{\mathrm{d}x}T_i(0)T_j'(0)\right),
\end{aligned}
\tag{26}
$$

where the $'$ symbol is used to represent the first derivative of the Chebyshev polynomial.

It is worth noting that almost all the integrals are frequency, flow, geometry and azimuthal order independent, which is a direct consequence of the chosen basis. They just need to be computed once and for all and can then be stored, thus allowing for fast computations. The integral $\int_0^1 \frac{1}{r+\frac{R_1}{R_2-R_1}}T_i(r)T_j(r)\mathrm{d}r$ is the only one that depends on the geometry and that would slow down the computation if directly computed. Here this issue is dealt with by computing estimates of this integral using a Gauss-Legendre quadrature in the radial direction.

IV. Validation for an infinite uniform duct

For an infinite lined annular uniform duct, the propagation problem reduces to the eigenvalue problem given in equation (17). The solution of this problem can then be used as the radiation boundary condition for varying ducts.

The test case parameters are taken from the literature. They are set to be representative of a modern engine inlet, with a unit nacelle radius R_2, a spinner radius R_1 equal to 0.3, a wall impedance Z_2 equal to $2-\mathrm{i}$ and a Mach number M of 0.5. The acoustic variables are computed at $\omega = 25$ and for an azimuthal mode $m = 24$ [21]. At first, both the distribution of the upstream eigenvalues in the complex plane and the shape of an upstream transverse function for the radial order $n = 5$ are given using a Chebyshev basis to show the capacity of this basis to correctly represents the physics. Then, to evaluate its interest over a standard hard-walled transverse basis, the decrease of the error with the increase of the number of basis functions is investigated using both bases. The evolution of the error on the radial eigenmode is defined by:

$$
\epsilon_p = \frac{\int_r |\Phi_p - \Phi_\infty|^2 r\mathrm{d}r}{\int_r |\Phi_\infty|^2 r\mathrm{d}r},
\tag{27}
$$

with Φ_p the potential obtained with p basis functions and Φ_∞ the reference analytical solution [3].

The eigenmode calculation associated with a radial mode order $n = 5$ for different numbers of polynomials is given in figures 1a and 1b. An excellent agreement is obtained when fifteen or twenty polynomials are used. However,

with few of them, the solution quickly deteriorates, and with ten polynomials, the radial structure of the mode is lost. To strengthen our analysis, a plot in the complex plane of the acoustic wavenumbers estimated with the eigenvalue resolution are given in figure 1c and are compared with the analytical solution. The conclusions are the same as the previous ones: when enough basis functions are used, they are only minor differences between the eigenvalues obtained numerically and the analytical ones. Note that this required number of basis functions is strongly dependent on the radial mode order.

The results of the convergence process carried out using the Chebyshev and hard-walled Bessel bases are given in figure 1d. As expected, the Chebyshev basis outperforms the Bessel one when many polynomials are used, with an exponential error decrease compared to a linear one. However, the hard-walled transverse eigenmodes better represent the real eigenmodes than the Chebyshev polynomials before a certain buffer. These results confirm that the method has excellent convergence and accuracy in resolving the BC if enough Chebyshev polynomials are used. For most cases, when $2n + 10$ polynomials are used, with n the biggest radial wavenumber order to represent, the results are weakly sensitive to the inclusion of further polynomials. Therefore, this criterion is ensured in the remaining of the paper to represent the physics correctly.

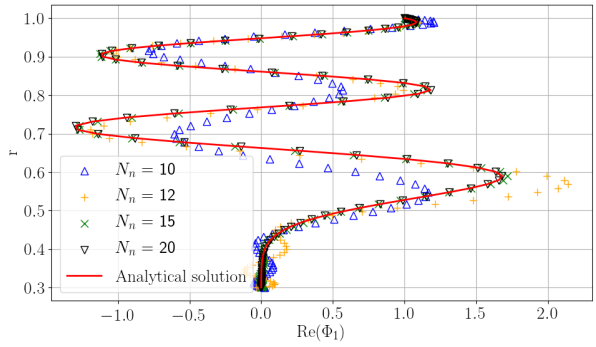

(a) Radial evolution of the eigenmode $n = 5$ (real part)

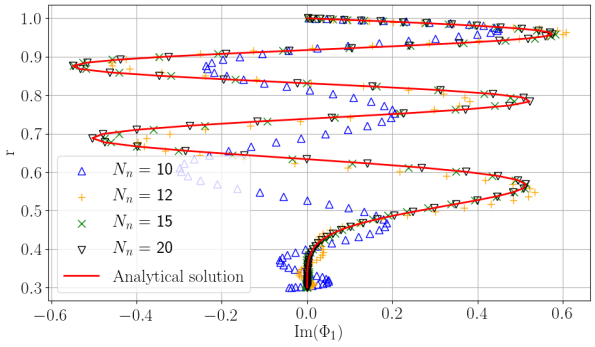

(b) Radial evolution of the eigenmode $n = 5$ (imaginary part)

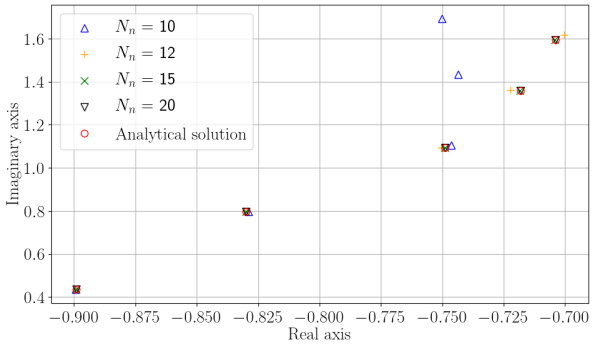

(c) First five radial computed eigenvalues in the complex plane

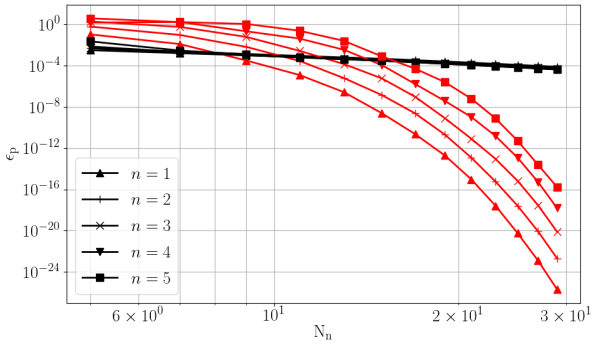

(d) Evolution of the error with the number of basis functions used with hard-walled Bessel functions (black lines) and Chebyshev polynomials (red lines)

Fig. 1 Validation of the eigenvalue resolution inside a constant waveguide with $(R_1, R_2) = (0.3, 1)$, $M = 0.5$, $\omega = 25$, $m = 24$ and $Z_2 = 2 - \mathrm{i}$.

V. Validation for a slowly varying duct

A. Validation methodology

1. Finite-element method

The numerical validation tool for ducts of varying cross-sections is based on finite-element method (FEM) [22]. This solver is used to compute both the steady potential flow and the acoustic field. It is based on a weak formulation of equations (1) and (2) over a volume V bounded by a surface S. These equations are written, for the mean flow:

$$\begin{gathered}\int_V D\nabla W\nabla\Phi_0 \mathrm{d}V = \int_S DW\nabla\Phi_0\cdot\mathbf{n}\mathrm{d}S,\\ D = \left((\gamma-1)\left(E-\frac{1}{2}\frac{\partial\Phi_0}{\partial x}^2-\frac{1}{2}\frac{\partial\Phi_0}{\partial r}^2\right)\right)^{1/(\gamma-1)},\\ C = D^{\frac{\gamma-1}{2}},\end{gathered} \tag{28}$$

and for the acoustics:

$$\begin{gathered}\int_V D\nabla W\cdot\nabla\Phi - \frac{D}{C^2}\left(\nabla\Phi_0\cdot\nabla\Phi+\mathrm{i}\omega\Phi\right)\left(\nabla\Phi_0\cdot\nabla W-\mathrm{i}\omega W\right)\mathrm{d}V =\\ \int_S DW\nabla\Phi\cdot\mathbf{n} - W\frac{D}{C^2}\left(\nabla\Phi_0\cdot\nabla\Phi+\mathrm{i}\omega\Phi\right)\nabla\Phi_0\cdot\mathbf{n}\mathrm{d}S,\end{gathered} \tag{29}$$

with Φ_0 the steady flow potential, W a continuous test function and $\mathbf{n}$ the outward-oriented normal. All the variables are the same as the ones used in section II.

Equation (28) is nonlinear and is solved using a Newton iterative algorithm [23]. At each iteration, the density and the speed of sound are derived from the value of the potential at the previous iteration. A mass flow is imposed at both ends of the duct.

For solving equation (29), it is necessary to define the boundary condition terms. They correspond to the right term of the linearized potential equation formulated as a variational statement. The boundary conditions are divided into fluid conditions (injection/exit) and wall conditions. For the boundary at the wall level, two cases are again distinguished: the hard-walled and the lined case. The hard-walled boundary condition ($\nabla\Phi\cdot\mathbf{n}=0$) is the easiest one to implement since there is no term to add to equation (29). The lined wall boundary condition is implemented using a simplified formulation. This boundary condition was proposed in [24] and assumes an infinitely thin boundary layer above the acoustic treatment. To implement this boundary condition, the following term is added to equation (29):

$$\nabla\Phi\cdot\mathbf{n} = \frac{\mathrm{D}}{\mathrm{D}t}\left(\frac{-D}{\mathrm{i}\omega Z}\frac{\mathrm{D}\phi}{\mathrm{D}t}\right),\quad \text{with } \frac{\mathrm{D}}{\mathrm{D}t} = \mathrm{i}\omega+\mathbf{V}\cdot\nabla. \tag{30}$$

For the injection/exit BC, a representation over transverse hard-walled modes is used. These conditions allow to specify the incoming mode and to avoid any reflection on the source/exit plane.

2. Test case geometry and flow conditions

For all the following test cases, a CFM56 engine will be used. This engine is here considered axisymmetric, so its geometry is entirely defined by the spinner radius R_1 and nacelle radius R_2. The values taken for these radii are [25]:

$$\begin{gathered}R_1(x) = \max\left(0, 0.64212-\left(0.04777+0.98234y^2\right)^{0.5}\right),\\ R_2(x) = 1-0.18453y^2+0.10158\frac{\mathrm{e}^{-11(1-y)}-\mathrm{e}^{-11}}{1-\mathrm{e}^{-11}},\\ 0\le x\le 2,\ y=x/L \text{ and } L=2.\end{gathered} \tag{31}$$

The fan is located at the axial position $x=0$ and the exit radiation condition is at $x=L$. For a turbofan engine in normal flight conditions, the flow goes from the exit to the fan and is driven by a mass flow condition at the fan level. Therefore

the flow characteristics are given there, with a zero or non zero axial velocity and a unit value for both the normalized density and speed of sound. Test cases with flow are performed with a Mach number of -0.5. The acoustic source is also located at the level of the fan and propagates against the flow. The shielding effect of the fan is not considered, and an infinite duct outlet condition is assumed, which means that the exit and the source planes have zero reflection coefficients.

3. Flow computation

For cases with flow, a value of $M = -0.5$ is specified at the level of the fan. Before computing the acoustics, the steady axial mean flow field and the velocity streamlines obtained when using the FEM are represented in figure 2a. The averaged axial velocity over successive cross-sections obtained is then compared with the flow computed by the MS method in figure 2b. Even if the mean axial velocity obtained with both methods is almost identical, the contours of axial velocity show that the vertical iso-contours prescribed by the MS assumption are not respected. This is particularly true near the exit ($x = L$) of the duct where the geometry is not slowly varying ($\epsilon \approx \mathrm{d}R_2/\mathrm{d}X \approx 0.3$).

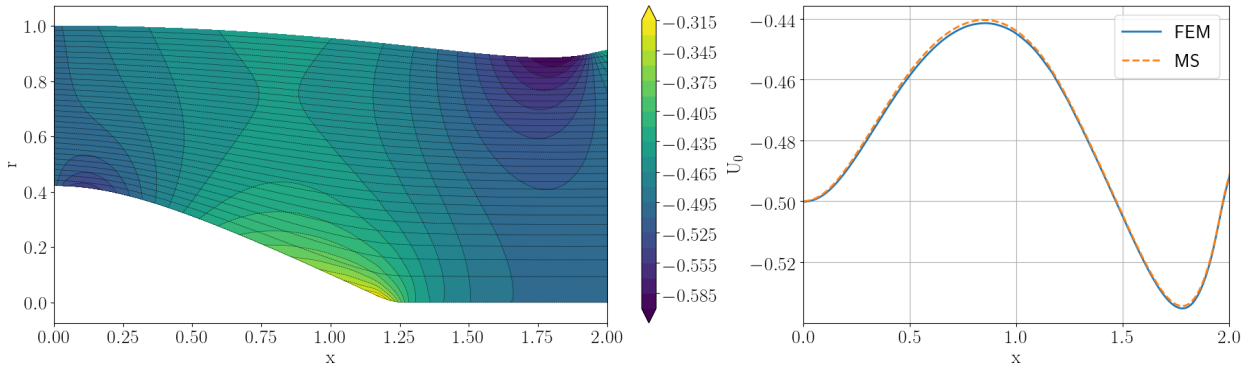

(a) Map of normalized axial velocity

(b) Mean normalized axial velocity obtained with the FEM solver (solid line) and with the MS approximation (dotted line)

Fig. 2 Flow computed for a specified Mach number $M = -0.5$ at $x = 0$.

4. Numerical discretization

Details about the numerical resolution are defined here and will be applied to all the test cases. For the developed MM, we need to define an axial discretization and a number of polynomials in the radial direction. The radial discretization is addressed in section IV and the $2n + 10$ criterion is kept. To be accurate when computing a mode, there is a need to have at least five times more points axially than the shortest convected wavelength. This last one is estimated by performing the calculation of the eigenvalues at each BC, as seen in section IV. With these criteria, all the test cases that will be presented took less than a second to run with the developed MM.

For the FEM, the field is interpolated on an unstructured, triangular mesh generated using Gmsh [26]. The acoustic potential field is approximated with second-order Lagrange polynomials. The axial discretization is the same as the one of the MM computation. In some specific cases (particularly with a liner), these meshes cannot correctly represent the acoustics, and a convergence mesh procedure has been carried out.

5. Numerical solutions

Several computations are performed to understand the strengths and weaknesses of the developed method. At first, calculations are done using the developed MM formulation for each test case. This method can be applied with two different bases (see section III.D), but the Chebyshev one is preferred since it gives shorter calculation times than the transverse eigenmode basis (Bessel). Nevertheless, the multimodal method is also used with the less-performing Bessel basis in hard-walled cases where the modal scattering can be artificially turn-off (see section III.D). In that cases, the problem reduces to a scalar integration which makes the calculation time low. This multimodal method without

scattering is referred to as MMWS in the following. Comparisons with the MM results (with Chebyshev basis) allow understanding the improvement brought by a formulation that captures the scattering mechanisms by which acoustic power leaks on adjacent eigenmodes.

In order to check that our method is correctly implemented and that the $O(\epsilon^2)$ terms neglected in equation (8) do not impact the solution, FEM computations are performed using the flow calculated with the MS approximation (referred to as FEM/MS). Finally, the method is evaluated against reference FEM solutions that use the exact flow (referred to as FEM/CFD).

B. Hard-walled cases

1. Test case parameters

Six test cases are done without wall acoustic treatment. They are taken to be realistic of modern aeroengines in terms of frequencies and circumferential mode numbers both with and without mean flow. These test cases can be divided into three categories: two standard cut-off modes, two standard cut-on modes, and two numerically-challenging cases where the injected mode encounters a transition inside the geometry. The intention is to explore both the model's capacity to represent the physics and the numerical stability of the implementation around a transition, which is a singularity of the admittance matrix. The non-dimensional parameters for each test case are listed in table 1.

Case	(m, n)	ω	Mach number	Mode behaviour
1	(10,1)	10	0	cut-off
2	(10,1)	10	-0.5	cut-off
3	(30,1)	50	0	cut-on
4	(30,2)	50	-0.5	cut-on
5	(20,7)	50.2	0	transition
6	(20,7)	44.4	-0.5	transition

Table 1 Summary of the hard-walled test case parameters.

2. Results

For all the presented test cases, iso-pressure contour plots over the meridional plane are given to represent the MM, the MMWS and the FEM results. These graphs are given in figures 3, 4, 5, 6, 7 and 8.

The first thing that appears is that the scattering is limited for all the test cases, and neglecting it seems to give consistent results. The simplified MMWS method perfectly captures total reflection phenomena, such as turning points caused by a transition. There is an almost perfect agreement in the cases without flow when adding the modal scattering to the multimodal formulation. This proves that the use of the admittance matrix allows to represent the reflection and refraction index of the medium and the intermodal exchange of energy. Note that the admittance admits a quasi-singularity for the transition case. However, the Magnus-Moebius scheme avoids numerical trouble, and the total reflection of the main mode at the turning point level is observed. When there is a flow, some discrepancies appear between all the methods. The FEM/MS and the MM results are still in good agreement, but they differ from the FEM/CFD ones. This means that the main cause of discrepancy is the flow estimation.

For the cut-off test case, the agreement of iso-pressure contours is still excellent, and the model perfectly captures the high attenuation of the mode. For this test case, there is almost no acoustic propagation in the region where the MS approximation of the flow is erroneous, which explains the observed agreement. For the cut-on case, as expected, the error between the reference solution and the MM solution is located in a region where the MS flow approximation starts to become erroneous ($|\mathrm{d}R_2/\mathrm{d}x| > 0.1$ for $1.7 < x < 2$). Surprisingly, the MMWS offers a better estimate of the pressure field in that region. This proves that a non-physical important modal flow-induced scattering at this location deteriorates the results. Note that this comes from the fact that the exact flow considers a constant duct at the outlet, which tends to reduce the values of the radial velocity when compared to the MS flow. Therefore, this geometry is unfavourable to the MM method, but we did not want to hide the method's weaknesses by modifying the geometry. However, the results are still in good agreement with the FEM/CFD solution elsewhere in the duct. For the transition case, a slight shift is visible

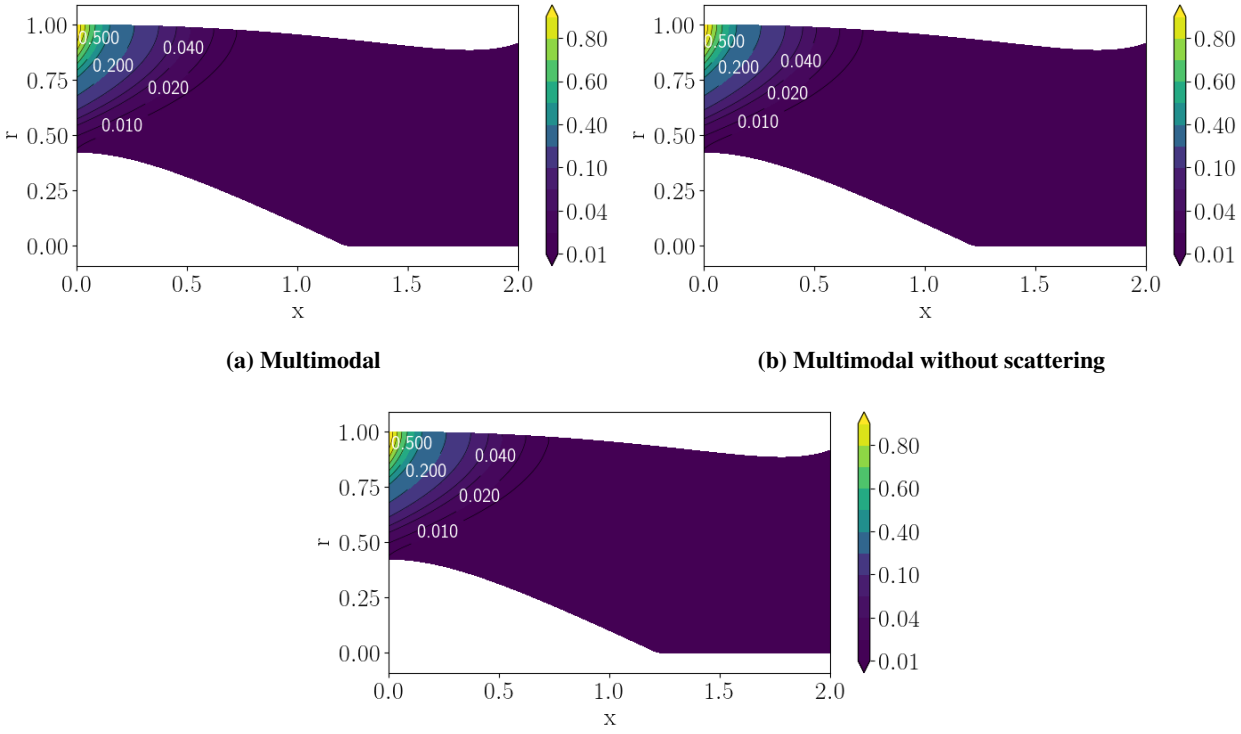

(a) Multimodal

(b) Multimodal without scattering

(c) Finite-element method

Fig. 3 Maps of absolute pressure associated to the mode (10,1) at $\omega = 10$ for $M = 0$.

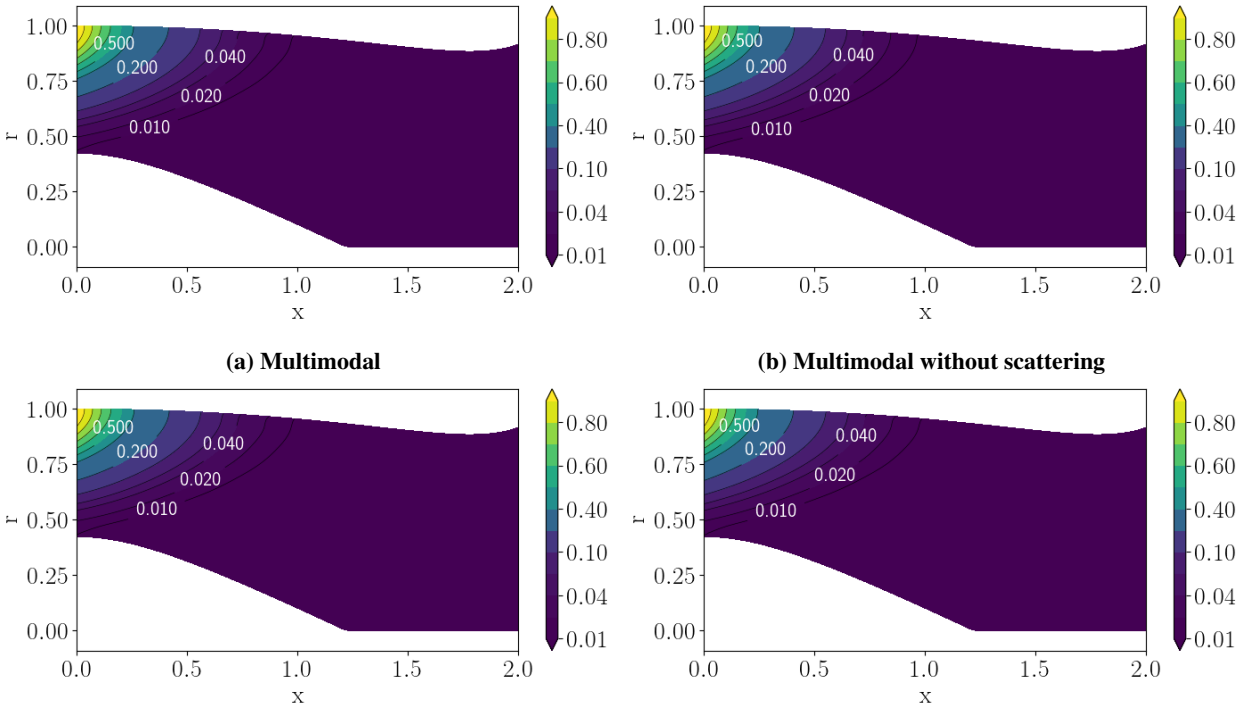

(a) Multimodal

(b) Multimodal without scattering

(c) Finite-element method with MS flow

(d) Finite-element method with CFD flow

Fig. 4 Maps of absolute pressure associated to the mode (10,1) at $\omega = 10$ for $M = -0.5$.

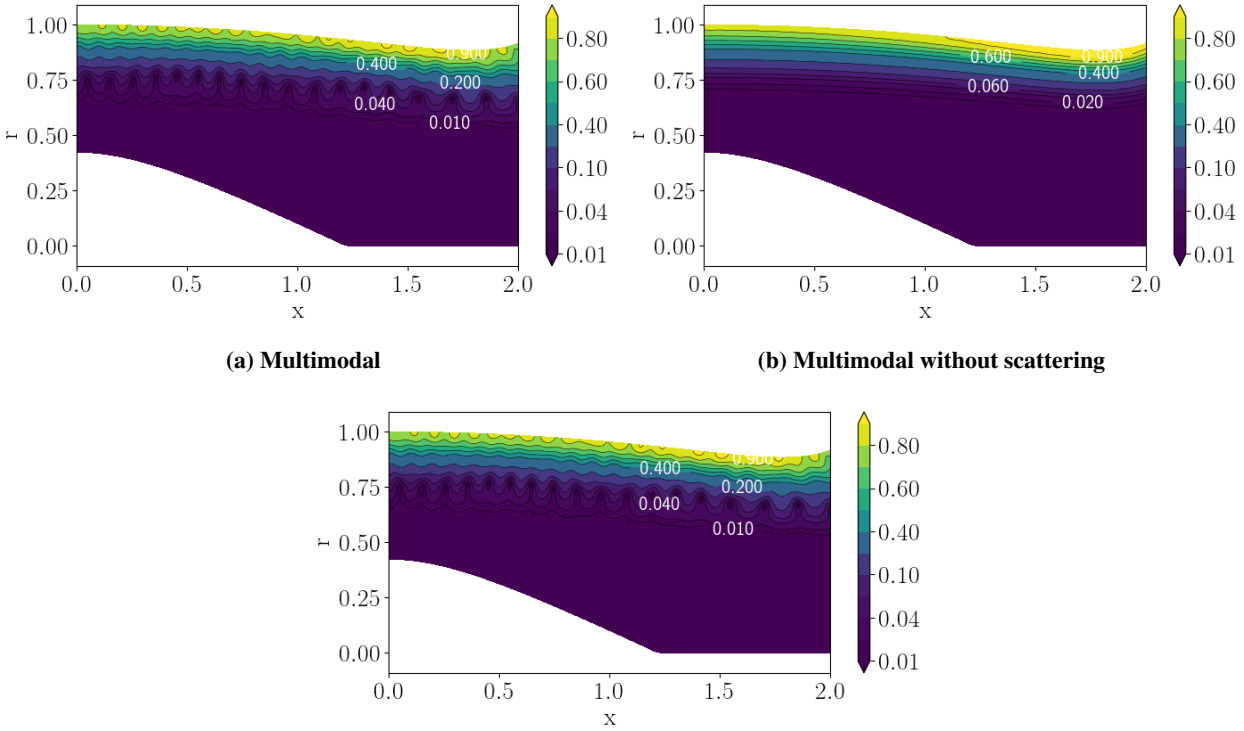

(a) Multimodal **(b) Multimodal without scattering**

(c) Finite-element method

Fig. 5 Maps of absolute pressure associated to the mode (30,1) at $\omega = 50$ for $M = 0$.

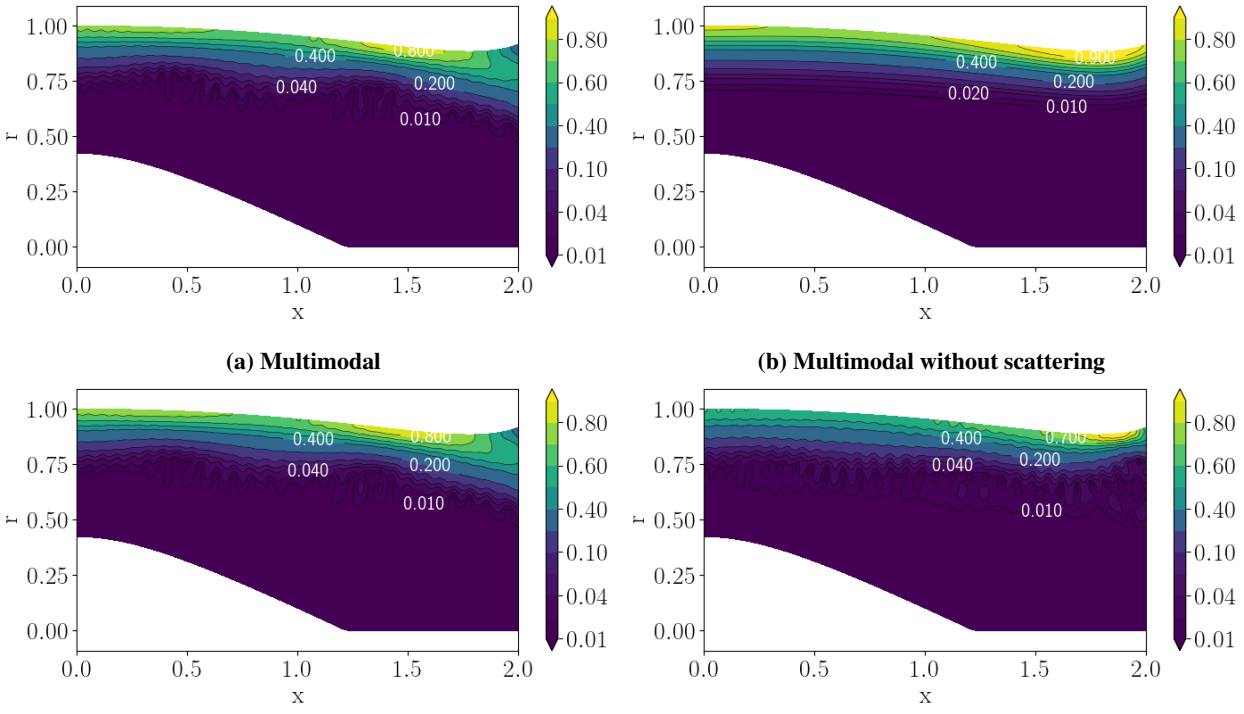

(a) Multimodal **(b) Multimodal without scattering**

(c) Finite-element method with MS flow **(d) Finite-element method with CFD flow**

Fig. 6 Maps of absolute pressure associated to the mode (30,1) at $\omega = 50$ for $M = -0.5$.

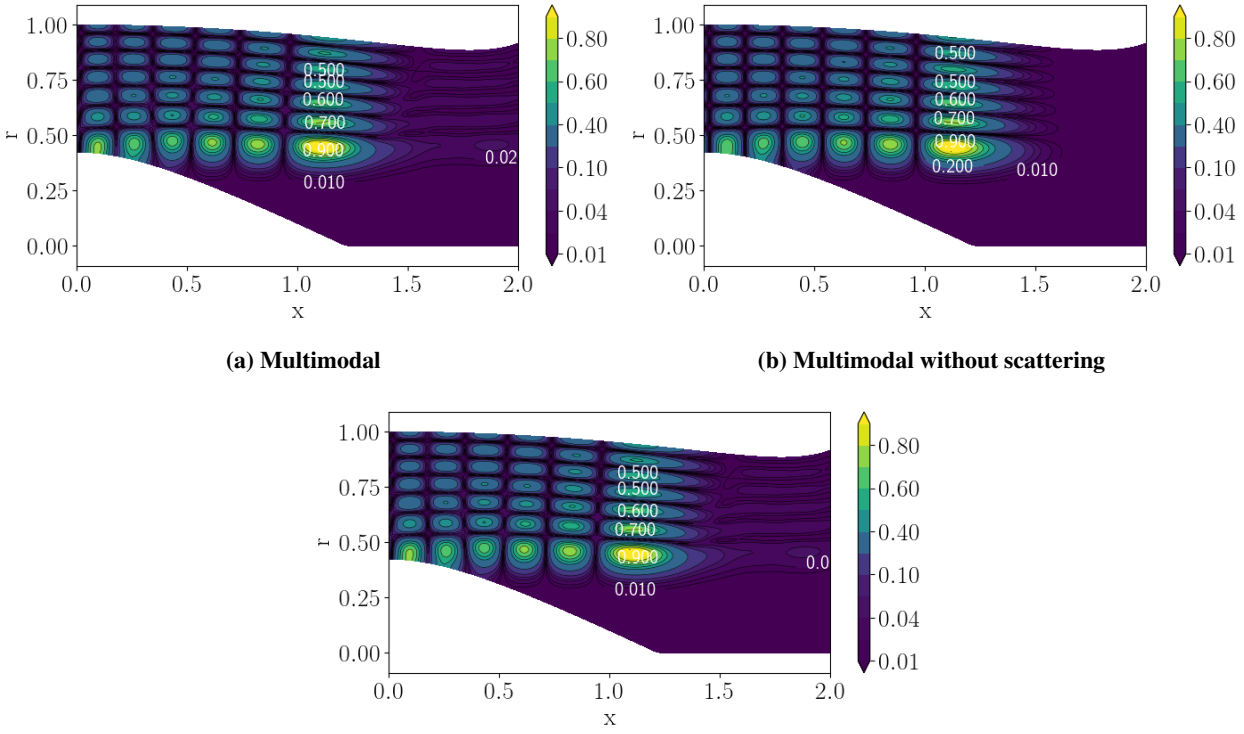

(a) Multimodal **(b) Multimodal without scattering**

(c) Finite-element method

Fig. 7 Maps of absolute pressure associated to the mode (20,7) at $\omega = 50.2$ for $M = 0$.

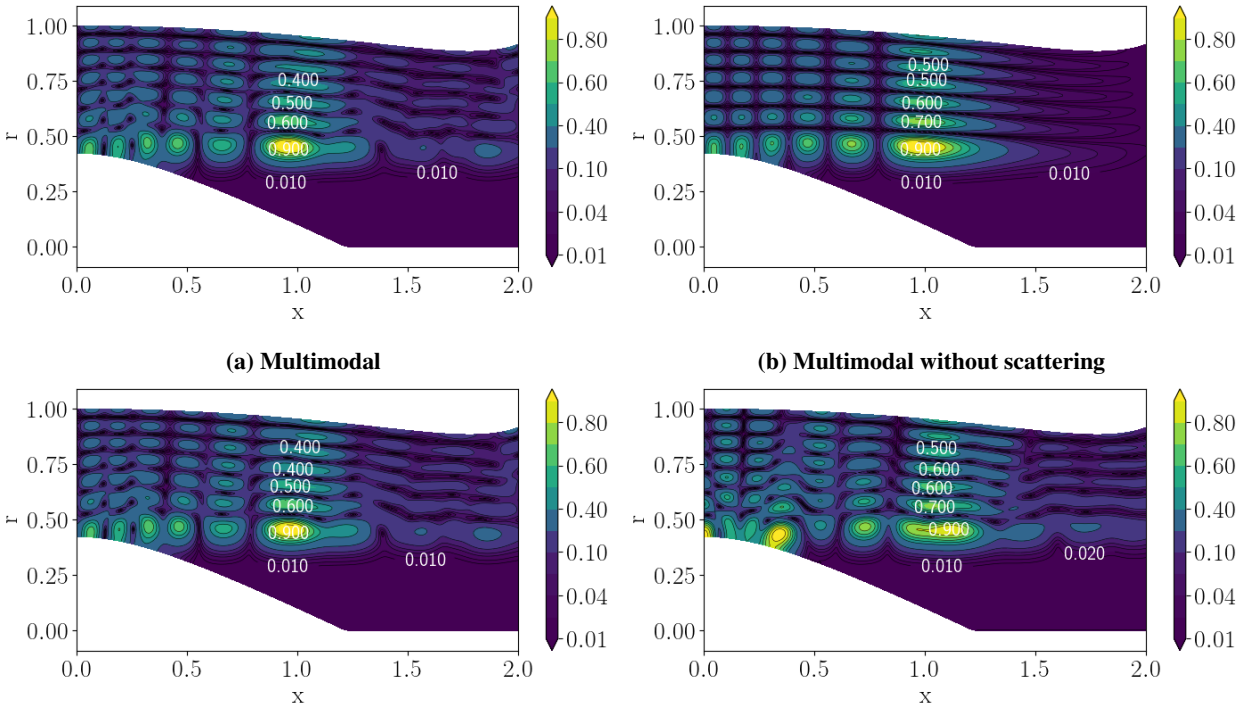

(a) Multimodal **(b) Multimodal without scattering**

(c) Finite-element method with MS flow **(d) Finite-element method with CFD flow**

Fig. 8 Maps of absolute pressure associated to the mode (20,7) at $\omega = 44.4$ for $M = -0.5$.

between the FEM/CFD and the MM solution, even in a region where the MS approximation should be satisfactory. This comes from the fact that transitions are very sensitive to small parameter changes so that even a tiny error on the flow estimate can change the response of the overall system [25].

Outside of the flow discrepancies that have been presented, other differences could impact the propagation. They could explain the minor differences observed between the FEM/MS and the multimodal results:

1) There is a difference between the FEM and the MM formulation at the duct exit, where the boundary conditions are coded differently. For the FEM, the output condition only imposes a continuity condition on the acoustic potential, whereas the MM also imposes a continuity condition on the axial velocity. For a wall slope that is non-zero at the exit, this could cause discrepancies.
2) Some parasitic refection can appear at the duct exit with the FEM formulation.
3) Some flow terms ($O(\epsilon^2)$) have been neglected in equation (8) for constructing the multimodal formulation.

C. Lined wall cases

1. Test case parameters

Ten test cases are done to validate the model for lined wall boundary conditions. The parameters are taken from the paper [27] in which a FEM method is compared to an analytical method. The same hypothesis that $Z_2 = 2 - \mathrm{i}$ does not vary with the frequency is assumed. Note that the sorting of the modes used here is not the same as in the reference paper, which uses an analogy to the cut-on ratio to sort modes. Here the sorting is based on the hard-walled equivalent sorting of the modes (by computing the trajectories of the eigenvalues in the complex plane).

The comparisons were performed on contour plots of absolute pressure for the hard-walled test cases. Here a more quantitative comparison is made by giving the power attenuation predicted by each method. These data are set to prove the MM capacity to estimate the liner's impact on the propagation. These test cases are distinguished into no-flow cases where we expect our model to be perfectly accurate and flow cases where it should give approximate results. However, the flow-induced scattering phenomena should be of an order of magnitude inferior to the impact of the liner, and the attenuation predicted by our model should still be reliable.

The same axial discretization is not used for these test cases with both methods. Indeed, the FEM solver seems to have more trouble representing the exponential decay caused by the liner, and for each case, a mesh convergence process needs to be carried out to have consistent results.

2. Results

The attenuation obtained with our method and both FEM computations is given for all the test cases in table 2. The first observation is that all the methods agree on the no-flow cases on the expected attenuation. It is worth noting that a dynamic of more than a hundred dB (case 9) can be estimated with the numerical solver. For the flow test cases, discrepancies appear between all methods (even the FEM/MS and MM results differ) and no global trend appears. Even if the agreement deteriorates when a liner is used, the method still estimates the expected attenuation correctly. The prediction rarely differs by more than 1dB from the reference FEM/CFD results.

To understand the reason behind this worsening, pressure plots associated with test case 2, where the MM results and the FEM/MS results differ the most, are given in figure 9. There is a good agreement in terms of iso-pressure contours. Even if the impact of the liner is overestimated with the multimodal method, no major contrasts are observed. Since the hard-walled test cases gave results in relatively good agreement, the errors probably come from the radial boundary conditions.

A plot of the mean axial velocity at the tip level is given in figure 10 to understand the impact of the flow approximation at the wall. The axial velocity estimated by the MS approximation at tip is far from the reference FEM solution, with a maximum relative error of 15%. This could explain the differences between the FEM/MS and FEM/CFD results. However, the FEM/MS and MM use the same flow. The differences between both methods may come from $O(\epsilon^2)$ terms that have been neglected in our formulation. Neglecting those terms is not problematic for surface integrals that tend to smooth the flow errors (MS approximation of the mean flow is correct). However, the $O(\epsilon^2)$ boundary terms that have been neglected in equation (8) seem to play a minor role.

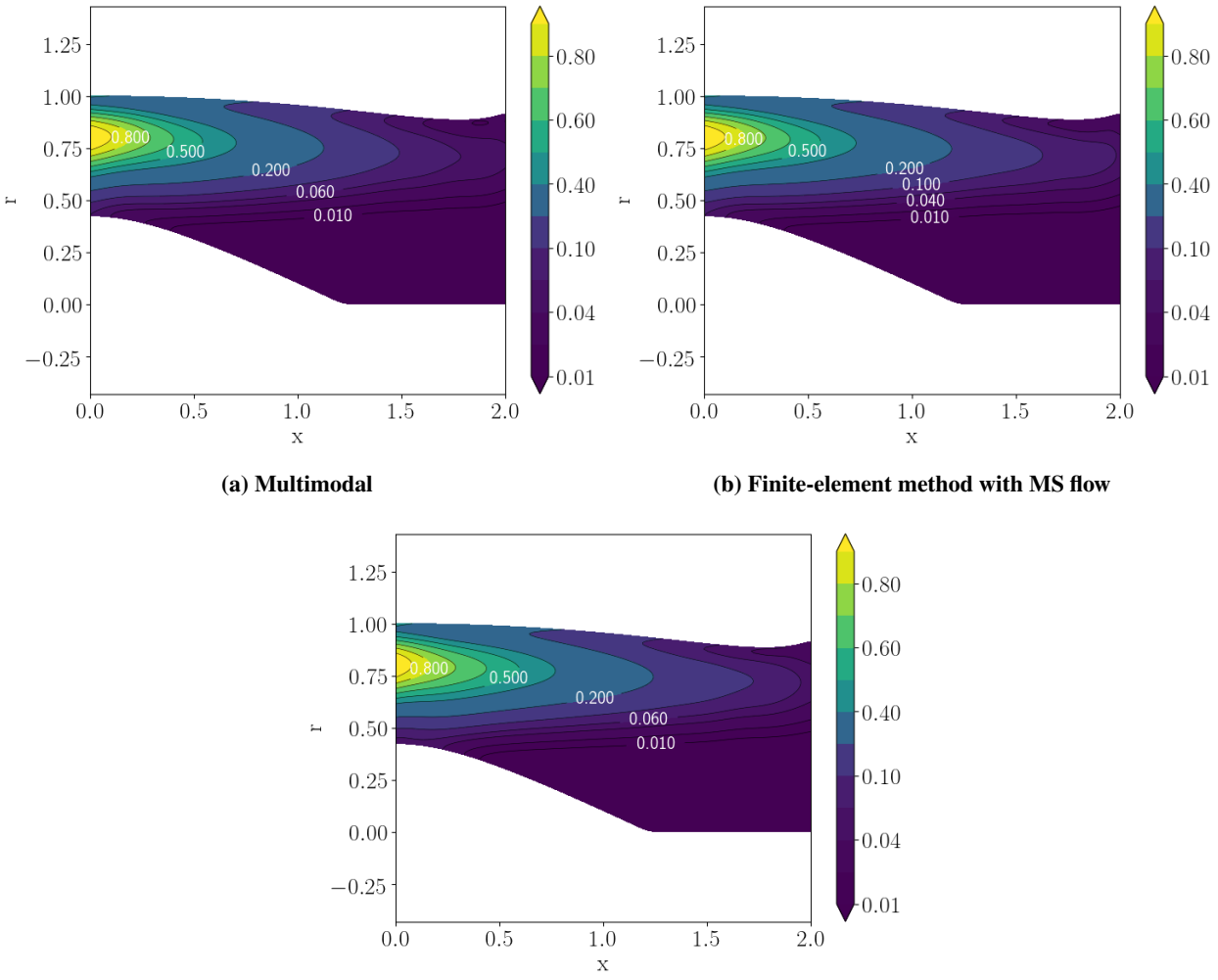

(a) Multimodal

(b) Finite-element method with MS flow

(c) Finite-element method with CFD flow

Fig. 9 Maps of absolute pressure associated to the mode (10,1) at $\omega = 16$ for $M = -0.5$ and $Z_2 = 2 - \mathrm{i}$.

Case	(m,n)	ω	Mach number	MM	FEM/MS	FEM/CFD
1	(10,1)	16	0	55.3 dB	55.3 dB	55.3 dB
2	(10,2)	16	-0.5	28.9 dB	26.7 dB	26.9 dB
3	(10,2)	50	0	4.9 dB	4.9 dB	4.9 dB
4	(10,2)	50	-0.5	2.0 dB	1.9 dB	1.5 dB
5	(20,2)	50	0	13.3 dB	13.3 dB	13.3 dB
6	(20,2)	50	-0.5	3.9 dB	3.7 dB	4.0 dB
7	(30,2)	50	0	30.8 dB	30.8 dB	30.8 dB
8	(30,2)	50	-0.5	9.5 dB	8.9 dB	9.9 dB
9	(40,2)	50	0	>150 dB	>150 dB	>150 dB
10	(40,2)	50	-0.5	30.1 dB	28.2 dB	29.0 dB

Table 2 Summary of the lined test case parameters and results.

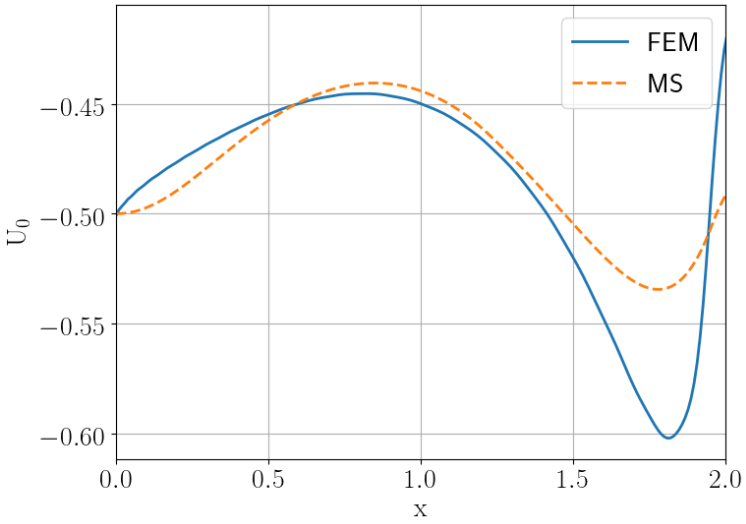

Fig. 10 Mean normalized axial velocity at tip obtained with the FEM solver and with the MS approximation.

VI. Conclusion

This paper presents a multimodal method applicable to the computation of the acoustic field in an axisymmetric duct with a multiple scales potential mean flow. The method uses a basis of Chebyshev polynomials, which proved to be effective at solving the wall boundary condition issue of most multimodal methods and allows extremely fast calculations. The method speed comes from the fact that almost all the radial integrations of the multimodal formulation are frequency, flow, geometry and azimuthal order independent.

Comparisons with a finite-element method which uses the same approximate flow, and one which uses an exact flow, have been carried out inside a turbofan engine over a large panel of flows and frequencies. The comparisons were made on pressure iso-contours, for the hard-walled test cases, and on power attenuations, for lined-wall cases. The agreement between the developed MM and the FEM that uses an approximate flow is excellent, but it deteriorates when the MM is compared to the FEM that uses an exact flow. Therefore, improving the flow representation would be necessary since some parasitic flow-induced scattering is present when using the MS approximation for flows with high Mach number. Still, the present multimodal formulation appears very efficient for studying propagation inside realistic turbofan engine inlets. It is particularly suited for fast evaluations of the attenuation expected from a liner inside varying ducts with a potential flow.

Another useful characteristic is the possibility to neglect the scattering mechanisms from the self-propagation of a mode in hardwalled-ducts when using the transverse eigenmode basis instead of the proposed basis based on Chebyshev polynomials. This allows extremely fast computations (integration of scalars) and permits knowing the best estimate that would give an analytical method that neglect modal scattering.

Note that the optimization of the numerical computation, particularly the search for an optimal number of Chebyshev polynomials to use, was not the purpose of this paper. The efficiency and numerical cost can be improved drastically by parallelizing the axial loop, but this appeared not to be necessary for a 2D geometry, with all the test cases running in less than a second. This paper demonstrates the efficiency of the multimodal method to compute acoustic propagation inside ducts with potential flows by showing that it could be done without increasing the computation time compared to no-flow multimodal methods. This work could be easily extended to more complex flows and geometries.

Acknowledgments

ONERA carried out these activities in the framework of the ADEC project. This project has received funding from the Clean Sky 2 Joint Undertaking within the European Union's Horizon 2020 research and innovation program, under grant agreement GA ID No. 945583 - LPA IADP 2020-2021.

References

[1] Pagneux, V., "Multimodal admittance method in waveguides and singularity behavior at high frequencies," *Journal of Computational and Applied Mathematics*, Vol. 234, No. 6, 2010, pp. 1834–1841. https://doi.org/10.1016/j.cam.2009.08.034.

[2] Gabard, G., "Noise sources for duct acoustics simulations: Broadband noise and tones," *AIAA Journal*, Vol. 52, No. 9, 2014, pp. 1994–2006. https://doi.org/10.2514/1.J052739.

[3] Goldstein, M. E., *Aeroacoustics*, McGraw-Hill International Book Company, 1976.

[4] Rienstra, S. W., "Sound transmission in slowly varying circular and annular lined ducts with flow," *Journal of Fluid Mechanics*, Vol. 380, 1999, pp. 279–296. https://doi.org/10.2514/6.1998-2311.

[5] Cooper, A. J., and Peake, N., "Propagation of unsteady disturbances in a slowly varying duct with mean swirling flow," *Journal of Fluid Mechanics*, Vol. 445, 2001, pp. 207–234. https://doi.org/10.1017/s0022112001005559.

[6] Peake, N., and Cooper, A. J., "Acoustic propagation in ducts with slowly varying elliptic cross-section," *Journal of Sound and Vibration*, Vol. 243, No. 3, 2001, pp. 381–401. https://doi.org/10.1006/jsvi.2000.3411.

[7] Brambley, E. J., and Peake, N., "Sound transmission in strongly curved slowly varying cylindrical ducts with flow," *Journal of Fluid Mechanics*, Vol. 596, 2008, pp. 387–412. https://doi.org/10.1017/S0022112007009603.

[8] Rienstra, S. W., "Slowly varying modes in a two-dimensional duct with shear flow and lined walls," *Journal of Fluid Mechanics*, Vol. 906, 2020. https://doi.org/10.1017/jfm.2020.687.

[9] Smith, A. F., Ovenden, N. C., and Bowles, R. I., "Flow and geometry induced scattering of high frequency acoustic duct modes," *Wave Motion*, Vol. 49, No. 1, 2011, pp. 109–124. https://doi.org/10.1016/j.wavemoti.2011.07.006.

[10] Wilson, A., "Propagation of acoustic perturbations in non-uniform ducts with non-uniform mean flow using eigen analysis in general curvilinear coordinate systems," *Journal of Sound and Vibration*, Vol. 443, 2019, pp. 605–636. https://doi.org/10.1016/j.jsv.2018.11.023.

[11] Pagneux, V., Amir, N., and Kergomard, J., "A study of wave propagation in varying cross-section waveguides by modal decomposition. Part I. Theory and validation," *The Journal of the Acoustical Society of America*, Vol. 100, No. 4, 1996, p. 2034. https://doi.org/10.1121/1.417913.

[12] Lu, Y. Y., "A fourth-order Magnus scheme for Helmholtz equation," *Journal of Computational and Applied Mathematics*, Vol. 173, No. 2, 2005, pp. 247–258. https://doi.org/10.1016/j.cam.2004.03.010.

[13] Félix, S., and Pagneux, V., "Multimodal analysis of acoustic propagation in three-dimensional bends," *Wave Motion*, Vol. 36, No. 2, 2002, pp. 157–168. https://doi.org/10.1016/S0165-2125(02)00009-4.

[14] Guennoc, T., Doc, J. B., and Félix, S., "Improved multimodal formulation of the wave propagation in a 3D waveguide with varying cross-section and curvature," *The Journal of the Acoustical Society of America*, Vol. 149, No. 1, 2021, pp. 476–486. https://doi.org/10.1121/10.0003336.

[15] Rienstra, S. W., "Fundamentals of Duct Acoustics, VKI Lecture Series 2016-02. Notes of course "Progress in Simulation, Control and Reduction of Ventilation Noise", November 16-18, 2015. ISBN-13 978-2-87516-098-0." Tech. rep., Technische Universiteit Eindhoven, 2016.

[16] Ingard, U., "Influence of Fluid Motion Past a Plane Boundary on Sound Reflection, Absorption, and Transmission," *The Journal of the Acoustical Society of America*, Vol. 31, No. 7, 1959, pp. 1035–1036. https://doi.org/10.1121/1.1907805.

[17] McTavish, J. P., and Brambley, E. J., "Nonlinear sound propagation in two-dimensional curved ducts: A multimodal approach," *Journal of Fluid Mechanics*, Vol. 875, 2019, pp. 411–447. https://doi.org/10.1017/jfm.2019.497.

[18] Canuto, C., Houssanini, M. Y., Quarteroni, A., and Zang, T. A., *Springer series in computational physics*, Springer, New York, 1988. https://doi.org/10.1016/0010-4655(84)90059-6.

[19] Boyer, G., Piot, E., and Brazier, J. P., "Theoretical investigation of hydrodynamic surface mode in a lined duct with sheared flow and comparison with experiment," *Journal of Sound and Vibration*, Vol. 330, No. 8, 2010, pp. 1793–1809. https://doi.org/10.1016/j.jsv.2010.10.035.

[20] Ralph Lewis, H., and Bellan, P. M., "Physical constraints on the coefficients of Fourier expansions in cylindrical coordinates," *Journal of Mathematical Physics*, Vol. 31, No. 11, 1990, pp. 2592–2596. https://doi.org/10.1063/1.529009.

[21] Astley, R. J., Sugimoto, R., Gabard, G., Norde, E., Grift, E. J., and Bocquier, M., "The effect of steady flow distortion on mode propagation in a turbofan intake," *20th AIAA/CEAS Aeroacoustics Conference*, 2014. https://doi.org/10.2514/6.2014-3113.

[22] Gabard, G., "PFE Software," , 2021. URL https://github.com/GwenaelGabard/pfe.

[23] Duta, M. C., and Giles, M. B., "A three-dimensional hybrid finite element/spectral analysis of noise radiation from turbofan inlets," *Journal of Sound and Vibration*, Vol. 296, No. 3, 2006, pp. 623–642. https://doi.org/10.1016/j.jsv.2006.03.006.

[24] Eversman, W., "The boundary condition at an impedance wall in a non-uniform duct with potential mean flow," *Journal of Sound and Vibration*, Vol. 246, No. 1, 2001, pp. 63–69. https://doi.org/10.1006/jsvi.2000.3607.

[25] Ovenden, N. C., Eversman, W., and Rienstra, S. W., "Cut-on cut-off transition in flow ducts: comparing multiple-scales and finite-element solutions," *10th AIAA/CEAS Aeroacoustics Conference*, 2004. https://doi.org/10.2514/6.2004-2945.

[26] Geuzaine, C., and Remacle, J. F., "Gmsh: A 3-D finite element mesh generator with built-in pre-and post-processing facilities," *International journal for numerical methods in engineering*, Vol. 79, No. 11, 2009, pp. 1309–1331. https://doi.org/10.1002/nme.2579.

[27] Rienstra, S. W., and Eversman, W., "A numerical comparison between multiple-scales and finite-element solution for sound propagation in lined flow ducts," *Journal of Fluid Mechanics*, Vol. 437, 2001, pp. 367–384. https://doi.org/10.2514/6.1999-1821.